AUTHOR QUERY FORM

ELSEVIER	**Journal: YJCPH** **Article Number: 4424**	**Please e-mail or fax your responses and any corrections to:** **E-mail: corrections.esch@elsevier.sps.co.in** **Fax: +31 2048 52799**

Dear Author,

Please check your proof carefully and mark all corrections at the appropriate place in the proof (e.g., by using on-screen annotation in the PDF file) or compile them in a separate list. Note: if you opt to annotate the file with software other than Adobe Reader then please also highlight the appropriate place in the PDF file. To ensure fast publication of your paper please return your corrections within 48 hours.

For correction or revision of any artwork, please consult http://www.elsevier.com/artworkinstructions.

Any queries or remarks that have arisen during the processing of your manuscript are listed below and highlighted by flags in the proof. Click on the 'Q' link to go to the location in the proof.

Location in article	Query / Remark: click on the Q link to go Please insert your reply or correction at the corresponding line in the proof
Q1 Q2	Please confirm that given names and surnames have been identified correctly. Please check the corresponding author e-mail addresses.
	Please check this box if you have no corrections to make to the PDF file ☐

Thank you for your assistance.
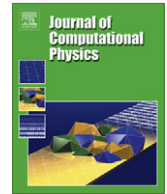
A weakly compressible free-surface flow solver for liquid–gas systems using the volume-of-fluid approach

Q1 Johan A. Heyns [a,*], Arnaud G. Malan [a], Thomas M. Harms [b], Oliver F. Oxtoby [a]

[a] Aerospace Systems Competency, Council for Scientific and Industrial Research, P.O. Box 395, Pretoria 0001, South Africa
[b] Mechanical and Mechatronic Engineering, University of Stellenbosch, South Africa

ARTICLE INFO

ABSTRACT

This paper presents a weakly compressible volume-of-fluid formulation for modelling immiscible high density ratio two-fluid flow under low Mach number conditions. This follows findings of experimental analyses that concluded the compressibility of the gas has a noteworthy effect on predicted pressure loads in liquid–gas flow in certain instances. With the aim of providing a more accurate numerical representation of dynamic two-fluid flow, the solver is subsequently extended to account for variations in gas densities. A set of governing equations is proposed, which accounts for the compressible properties of the gas phase in a manner which allows for a computationally efficient numerical simulation. Furthermore, the governing equations are numerically expressed so that they allow for large variations in the material properties, without introducing notable non-physical oscillations over the interface. For the discretisation of the governing equations an edge-based vertex-centred finite volume approach is followed. The developed solver is applied to various test cases and demonstrated to be efficient and accurate.

© 2013 Published by Elsevier Inc.

1. Introduction

As computational hardware and modelling techniques improve, the fidelity of numerical models increase along with their ability to model more complex flow phenomena with greater efficiency. One of the fields that enjoys continuous interest is the modelling of immiscible two-fluid flow or free-surface modelling (FSM) as it is commonly referred to. Examples of industries that benefit from accurate modelling of dynamic two-fluid flow include: The casting industry; maritime and naval engineering (where impact loads on fixed and floating structures are studied); as well as the transportation of fuel and other fluids by means of surface or air.

To date, most free-surface models treat both gas and liquid as incompressible [1–4], neglecting the effect of density changes due to pressure variations in the fluid. Though this is a reasonable assumption for most free-surface flow regimes, with high density ratio systems entrapped gas pockets may be subjected to notable fluctuations in pressure. Therefore, in these cases the compressibility of the gas cannot be neglected as it would influence the predicted pressures.

In a sensitivity analysis of two-fluid sloshing, [5] concluded that under near resonant conditions the inclusion of the compressibility of the gas has an noteworthy effect on the predicted pressure loads. Furthermore, experiments conducted by [6] as well as [7] showed that the compressibility of air has a significant effect on the impact pressures measured during

Q2 * Corresponding author.
E-mail addresses: jaheyns@gmail.com, jheyns@csir.co.za (J.A. Heyns), arnaud.malan@uct.ac.za (A.G. Malan), tmh@sun.ac.za (T.M. Harms), ooxtoby@csir.co.za (O.F. Oxtoby).

sloshing on the tank walls. They note that the presence of the compressible air reduces the peak pressure levels, but increases the duration of impact.

Various authors ([9–11]) have presented high fidelity compressible multi-fluid models. These typically employ the seven equation Baer–Nunziato type model, where two-fluid flow is described by two continuity equations, two momentum equations, two energy equations and a topological or interface equation. It is noted that with liquid–gas systems the material properties may vary by three orders of magnitude, introducing large discontinuities over the interface. Furthermore, for low Mach number flows, the time scales permitted for long wavelength acoustic wave propagation is not aligned with the physical time scales typically of interest. Using the above cited high fidelity approach to model low Mach number liquid–gas systems for an extended period of time is, therefore, deemed computationally overly expensive.

To account for the compressibility of single phase low Mach number flow, [12] presented a weakly compressible formulation. By means of a non-dimensional analysis the governing equations were reconstructed and only the dominant terms retained, allowing for a computationally efficient formulation. [13] subsequently applied this approach to an averaged two-fluid free-surface model and used a single compressibility parameter to describe the two fluids. The compressibility parameter is, however, a function of the square of the acoustic velocity and for liquid–gas systems may vary by an order of magnitude, introducing a discontinuity in the temporal term over the interface. In passing it is noted that though [14,15] have presented a weakly compressible formulation for free-surface flows; their formulations, however, only account for the liquid and neglects the description of the low density gas.

This work endeavours to extend on the above work and to this end presents a weakly compressible volume-of-fluid (VOF) formulation for modelling immiscible liquid–gas flow under low Mach number conditions. A set of volume-of-fluid governing equations are proposed that describe the flow of an immiscible liquid–gas system and accounts for the compressible properties of the gas phase. The formulation furthermore allows the solution to be free from significant non-physical oscillations when large differences in material properties are considered.

For spatial discretisation purposes, a compact stencil, edge-based finite volume approach is followed which is shown to be accurate as well as computationally efficient ([16–18]), while being applicable to hybrid unstructured meshes. Furthermore, the VOF approach in conjunction with an existing blended higher resolution surface capturing scheme ([19,20]) can be used to describe the evolution of the free-surface interface. For solution purposes, an efficient implicit matrix free methodology is employed. Finally, the developed formulation is evaluated via the application to a number of test cases.

2. Weakly compressible liquid–gas solver

If an Eulerian volume-of-fluid approach ([21]) is followed, a control volume partially filled with liquid and gas can be considered, where the volume fraction occupied by the liquid and the gas are respectively denoted α_l and α_g. The averaged liquid and gas volume fractions for an arbitrary cell ξ are respectively calculated using the volume ratios, $\alpha_l = V_l/V_\xi$ and $\alpha_g = V_g/V_\xi$. Furthermore, for this work a homogeneous flow model is employed, which assumes a cell-averaged velocity and pressure, so that in a given cell $u_l = u_g = u$ and $p_l = p_g = p$ hold. [22] et al. [22] explain that an averaged velocity can be assumed if the time scales on which the turbulent drag forces equalise the velocity are much smaller than the time scales on which the flow is averaged.

Considering the low Mach number application of this work, a weakly compressible formulation which assumes barotropic compression and expansion of the fluids is employed. Based on these assumptions, the continuity and momentum equations of respectively the liquid and gas simplify to read

$$\frac{\partial(\alpha_l \rho_l)}{\partial t} + \frac{\partial(\alpha_l \rho_l u_j)}{\partial x_j} = 0 \tag{1}$$

$$\frac{\partial(\alpha_l \rho_l u_i)}{\partial t} + \frac{\partial(\alpha_l \rho_l u_i u_j)}{\partial x_j} + \frac{\partial(\alpha_l p)}{\partial x_i} = S_l^i \tag{2}$$

$$\frac{\partial(\alpha_g \rho_g)}{\partial t} + \frac{\partial(\alpha_g \rho_g u_j)}{\partial x_j} = 0 \tag{3}$$

$$\frac{\partial(\alpha_g \rho_g u_i)}{\partial t} + \frac{\partial(\alpha_g \rho_g u_i u_j)}{\partial x_j} + \frac{\partial(\alpha_g p)}{\partial x_i} = S_g^i \tag{4}$$

where ρ_l and ρ_g represent respectively the density of the liquid and the gas, and u_j denotes the averaged cell velocity in the coordinate direction j. The compatibility relation for the volume fractions is $\alpha_l + \alpha_g = 1$ and the liquid and gas volume fractions can, therefore, be expressed as $\alpha_l = \alpha$ and $\alpha_g = (1 - \alpha)$. The source terms, $\mathbf{S}_l$ and $\mathbf{S}_g$, contain the hydro-static pressure terms as well as the viscous terms. If Newtonian flow is assumed then the following holds

$$S_l^i = \alpha \rho_l g_i + \frac{\partial}{\partial x_j}\left(\alpha \mu_l \frac{\partial u_i}{\partial x_j}\right) \tag{5}$$

$$S_g^i = (1 - \alpha)\rho_g g_i + \frac{\partial}{\partial x_j}\left((1 - \alpha)\mu_g \frac{\partial u_i}{\partial x_j}\right) \tag{6}$$

where μ denotes viscosity.

By adding Eq. (2) and Eq. (4) an averaged momentum equation for homogenous two-fluid flow is found

$$\frac{\partial(\rho u_i)}{\partial t} + \frac{\partial(\rho u_i u_j)}{\partial x_j} + \frac{\partial p}{\partial x_i} = S_i \tag{7}$$

where the mixture density and dynamic viscosity, expressed in terms of the volume fraction, are

$$\rho = \alpha \rho_l + (1 - \alpha)\rho_g$$
$$\mu = \alpha \mu_l + (1 - \alpha)\mu_g$$

From the isentropic relation for the speed of sound, $c_l^2 = \partial p/\partial \rho_l$, and by using the product rule, the liquid continuity Eq. (1) can be expanded and written as

$$\frac{\alpha}{c_l^2}\frac{\partial p}{\partial t} + \frac{\alpha u_j}{c_l^2}\frac{\partial p}{\partial x_j} + \rho_l\left[\frac{\partial \alpha}{\partial t} + \frac{\partial \alpha u_j}{\partial x_j}\right] = 0 \tag{8}$$

To evaluate the order of each term's contribution, Eq. (8) is cast into a non-dimensional form. The reference values for pressure, $\rho_o u_o^2$, density, ρ_o, velocity, u_o, time, t_o, and length, l_o yield the non-dimensional form

$$\alpha S M_l^2 \frac{\partial p^*}{\partial t^*} + \alpha M_l^2 u^* \frac{\partial p^*}{\partial x^*} + \rho_l^*\left[S\frac{\partial \alpha^*}{\partial t} + \frac{\partial \alpha^* u_j^*}{\partial x_j}\right] = 0 \tag{9}$$

where * denotes the non-dimensional quantities and $M_l = u_o/c_l$ is the liquid Mach number and $S = l_o/u_o t_o$ is the Strouhal number.

For low Mach number liquid–gas systems it is noted that the square of the liquid Mach number, M_l^2, is of order 10^{-7}. If the reference density, ρ_o, is taken to be of the same order as the gas density, the term ρ_l^* would be of order 10^3. It is, therefore, acceptable to neglect the first two terms of Eq. (8) and as the liquid density will always be non-zero the following holds

$$\frac{\partial \alpha}{\partial t} + \frac{\partial(\alpha u_j)}{\partial x_j} = 0 \tag{10}$$

which is similar to the VOF equation for incompressible FSM.

Next, the product rule is again applied to the gas continuity Eq. (3) and by rearranging the terms the following expression is found

$$(1 - \alpha)\frac{\partial \rho_g}{\partial t} + (1 - \alpha)u_j\frac{\partial \rho_g}{\partial x_j} + \rho_g\frac{\partial u_j}{\partial x_j} - \rho_g\left[\frac{\partial \alpha}{\partial t} + \frac{\partial(\alpha u_j)}{\partial x_j}\right] = 0 \tag{11}$$

where the last term in square brackets is the volume fraction Eq. (10) and equal to zero.

As pointed out previously, [12] presented a weakly compressible formulation for single phase flow with low Mach numbers. They showed via a non-dimensional analysis that in the expanded continuity equation the spatial derivative of pressure is negligibly small. A similar approach can be followed here by casting the equation given above into its non-dimensional form and evaluating the contribution of the respective terms. Again, from the isentropic relation for speed of sound, $c_g^2 = \partial p/\partial \rho_g$, it follows

$$\frac{(1 - \alpha)}{c_g^2}\frac{\partial p}{\partial t} + \frac{(1 - \alpha)u_j}{c_g^2}\frac{\partial p}{\partial x_j} + \rho_g\frac{\partial u_j}{\partial x_j} = 0 \tag{12}$$

with the non-dimensional version reading

$$(1 - \alpha)S M_g^2 \frac{\partial p^*}{\partial t^*} + (1 - \alpha)M_g^2 u_j^*\frac{\partial p^*}{\partial x_j^*} + \rho_g^*\frac{\partial u_j^*}{\partial x_j^*} = 0 \tag{13}$$

where $M_g = u_o/c_g$ is the gas Mach number and the square of M_g is of the order 10^{-6}. As previously noted, the reference density is of the same order as the gas density and ρ_g^* is therefore of order unity. When considering low Mach number liquid–gas systems, the order of the terms would suggest that the contribution of the spatial derivative of pressure to the gas density can be neglected. When modelling the high frequency pressure oscillations during the compression and expansion of entrapped gas pockets, relatively small time scales are required. If, however, larger length scales are considered, the effect of the temporal term cannot be neglected due to the increased contribution of the Strouhal number. From the non-dimensional analysis the gas continuity equation for weakly compressible flow thus simplifies to

$$\frac{(1 - \alpha)}{\rho_g}\frac{\partial \rho_g}{\partial t} = -\frac{\partial u_j}{\partial x_j} \tag{14}$$

which also holds for the incompressible liquid phase as it then reads $\partial u_i/\partial x_i = 0$.

For the weakly compressible formulation the barotropic compression and expansion of the gas can be approximated using a linear form of the ideal gas law

$$\rho_g - \rho_{go} = \frac{1}{c_g^2}(p - p_o) \tag{15}$$

where ρ_{go} and p_o is the initial gas density and pressure.

Following the non-dimensional analysis, it is implied that the effect of the pressure gradient in the gas phase on the gas density is negligible. To ensure consistency in the momentum equation, it is required that the hydro-static source term in the gas phase be neglected. This is, however, acceptable as the hydro-static pressure is a function of the density, which for the gas is up to three orders of magnitude smaller than the hydro-static pressure of the liquid.

To conclude, the proposed weakly compressible VOF equations describing low Mach-number liquid–gas flow read

$$\frac{\partial \alpha}{\partial t} + \frac{\partial(\alpha u_j)}{\partial x_j} = 0 \tag{16}$$

$$\frac{(1-\alpha)}{\rho_g}\frac{\partial \rho_g}{\partial t} = -\frac{\partial u_j}{\partial x_j} \tag{17}$$

$$\frac{\partial(\rho u_i)}{\partial t} + \frac{\partial(\rho u_i u_j)}{\partial x_j} + \frac{\partial p}{\partial x_i} = \frac{\partial}{\partial x_j}\left(\mu \frac{\partial u_i}{\partial x_j}\right) + \rho_l g_i \tag{18}$$

The formulation takes into consideration changes in gas density due to variations in pressure, describing both fluids and accounts for differences in the liquid–gas material properties. Apart from neglecting the gas hydrostatic pressure contribution, only the continuity equation differs from the incompressible VOF formulation as it now contains a conditional temporal term. As the conditional temporal term is only activated in the gas phase, it results in a discontinuity in the velocity gradient.

3. Numerical flow solver

In this section a general introduction to the finite volume, vertex centred, edge-based approach is presented. For a more detailed discussion of the spatial discretisation it is asked that the reader refers to the work of [17]. The weakly compressible FSM formulation derived previously can be described with a single unified governing equation

$$\mathbf{A}\frac{\partial \mathbf{W}}{\partial t} + \frac{\partial \mathbf{F}^j}{\partial x_j} - \frac{\partial \mathbf{G}^j}{\partial x_j} = \mathbf{S} \tag{19}$$

where

$$\mathbf{W} = \begin{pmatrix} \alpha \\ \rho_g \\ \rho u_i \end{pmatrix}, \quad \mathbf{F}^j = \begin{pmatrix} \alpha u_j \\ u_j \\ \rho u_i u_j + \delta_{ij} p \end{pmatrix}, \quad \mathbf{G}^j = \begin{pmatrix} 0 \\ 0 \\ \mu \frac{\partial u_i}{\partial x_j} \end{pmatrix},$$

$$\mathbf{A} = \begin{pmatrix} 0 \\ \frac{1-\alpha}{\rho_g} \\ 0 \end{pmatrix}, \quad \mathbf{S} = \begin{pmatrix} 0 \\ 0 \\ \rho_l g_i + S_i \end{pmatrix}$$

With the said finite volume approach, the spatial domain, $\mathcal{V}$, is subdivided into a finite number of non-overlapping volumes $\mathcal{V}_\xi \in \mathcal{V}$. The dual-mesh construction for the vertex-centred approach as proposed by [21] is illustrated in Fig. 1. By integrating over the finite volume, $\mathcal{V}_\xi$, the governing equation can be cast into the integral form and from the divergence theorem can subsequently be written in terms of surface integrals

$$\int_{\mathcal{V}_\xi} \mathbf{A}\frac{\partial \mathbf{W}}{\partial t}d\mathcal{V} + \int_{\mathcal{A}_\xi} (\mathbf{F}^j - \mathbf{G}^j)n_j d\mathcal{A} = \int_{\mathcal{V}_\xi} \mathbf{S}d\mathcal{V} \tag{20}$$
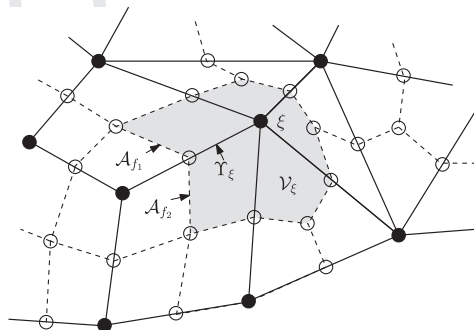

Fig. 1. Schematic of the median-dual-mesh construction on hybrid grids.

195 where $\mathcal{A}_\xi$ is the surface bounding $\mathcal{V}_\xi$ and **n** is the unit vector normal to the boundary segment $\mathcal{A}$ pointing outward.

196 To exploit the computational advantages of an edge-based assembly, the bounding surface information is stored in an

197 edge-wise manner, as edge-coefficients, which is defined as

$$\mathbf{C}_f = \mathbf{n}_{f_1}\mathcal{A}_{f_1} + \mathbf{n}_{f_2}\mathcal{A}_{f_2} \tag{21}$$

201 where f denotes the face value.

3.1. Volume-of-fluid approach

203 The volume-of-fluid or liquid continuity Eq. (10) remains unchanged from the incompressible FSM formulation

204 ([20]) and is, therefore, solved using a blended High-Resolution Artificial Compressive (HiRAC) formulation ([HiR-

205 AC employes a Jacobi type dual time stepping formulation with second-order Crank–Nicholson for the temporal discretisation

206 of the VOF equation. It also introduces an artificial compressive term (which is only activated in the interface to reduce

207 the numerical smearing associated with the VOF method. The semi-discrete form of the VOF equation reads

$$\frac{\alpha^{\tau+1} - \alpha^\tau}{\Delta t_\tau} = -\frac{1}{2}\left[\frac{\partial(u_i\alpha)}{\partial x_i}\bigg|^\tau + \frac{\partial(u_i\alpha)}{\partial x_i}\bigg|^n\right] - \frac{\partial}{\partial x_i}(u_c|_i\alpha(1-\alpha))|^\tau - \frac{\alpha^\tau - \alpha^n}{\Delta t} \tag{22}$$

211 where Δt_τ is the pseudo-time step size and u_c is the compressive velocity which acts normal to the free-surface interface. The

212 volume fraction face value, α_f, is discretised using a blended high-resolution scheme , switching between compressive

213 and higher resolution schemes based on the alignment of the free surface interface and the edge face. The combination of the

214 higher-resolution scheme and the addition of an artificial term reduces numerical diffusivity, ensuring a sharp interface is

215 maintained, while the integrity of the interface shape is preserved.

216 It should, however, be noted that according to Godunov's theorem no linear convection scheme of second-order accuracy

217 or higher can be monotonic . Therefore, to maintain a bounded solution, non-linear higher-resolution schemes employ

218 second-order interpolation in regions with smooth gradients, but revert back to first-order interpolation when sharp changes

219 in the gradient are encountered ([27]). This results in the accuracy of VOF schemes varying between first- and second-

220 order.

3.2. Split solver with artificial compressibility

222 For incompressible flow, proposed a matrix-free solver which combines the projected pressure (PP) method

223 and the artificial compressibility (AC) approach . It is said to provide the stability and robustness of the PP method

224 while retaining the computational efficiency of the AC approach. The split solver with AC was extended for application to

225 edge-based finite volume by .

226 Following a similar procedure, the continuity and momentum equations are solved using an upwind-stabilised pressure-

227 projection split with artificial compressibility. It is found that by employing the pressure-projection split with non-linear

228 higher-order upwind interpolation of the face fluxes sufficient numerical diffusion is introduced to ensure a stable solution.

229 Furthermore, by employing a Jacobi-type dual time-stepping approach the velocity, pressure and volume fraction is solved in

230 a fully coupled manner. The solver consists of three steps, first an intermediate momentum equation, from which the pres-

231 sure gradients are removed, is solved viz.

$$\frac{\Delta \rho u_i^*}{\Delta t} = -\frac{\partial(\rho u_i u_j)}{\partial x_j}\bigg|^\tau + \mu\frac{\partial}{\partial x_j}\left(\frac{\partial u_i}{\partial x_j}\right)^\tau \tag{23}$$

235 where $\Delta \rho u_i^* = \rho u_i^* - \rho u_i|^n, \Delta t = t^\tau - t^n$ and t^τ denotes dual time-stepping pseudo time.

236 Next, the pressure is calculated using an implicit pressure–projection equation with artificial compressibility

$$\frac{1}{c_\tau^2}\frac{p^{\tau+1} - p^\tau}{\Delta t_\tau} = -\frac{\partial}{\partial x_j}\left[u_j^\tau + \Delta u_j^* + \frac{\Delta t}{\rho}\left(-\frac{\partial p^{\tau+1}}{\partial x_j} + \alpha\rho_l g\right)\right] - \frac{(1-\alpha)}{\rho_g}\frac{1}{c_g^2}\frac{p^{\tau+1} - p^n}{\Delta t} \tag{24}$$

240 where c_τ is the artificial acoustic velocity and Δt_τ the pseudo time step size. The artificial acoustic velocity is calculated as

241 proposed by [33].

242 Finally, the velocities are calculated from the corrected momentum equation which contain the updated values

$$\frac{\rho u_i^{\tau+1} - \rho u_i^\tau}{\Delta t_\tau} = \frac{\Delta \rho u_i^*}{\Delta t} - \frac{\partial p^{\tau+1}}{\partial x_i} + \alpha\rho_l g - \frac{\rho u_i^\tau - \rho u_i^n}{\Delta t} \tag{25}$$

246 where equation tends to the implicit solution as it converges in pseudo time.

247 To improve the solution convergence rate the pressure-projection equation is solved using a Generalised Minimal Resid-

248 ual (GMRES) algorithm with Lower–Upper Symmetric Gauss–Seidel (LU–SGS) preconditioning [34,35].

3.3. Treatment of discontinuities in the spatial derivatives

Löhner et al. [3] note that if the density of the liquid and gas varies significantly, small changes in the pressure gradient over the interface will induce inaccurate acceleration of the gas. This consequently results in the formation of spurious oscillations in the velocity field over the interface. To overcome this [3] discretised the spatial pressure derivative in a piecewise linear manner. They noted that for incompressible free-surface flow the velocity field is continuous throughout the domain, so that for a given edge, Υ,

$$\frac{1}{\rho}\frac{\partial p}{\partial x}\bigg|_{\Upsilon} \approx c \tag{26}$$

In Eq. (26) the edge face value of the pressure is calculated using a piece-wise linear approximation, while the density is treated as a nodal value which is interpolated in a stepwise manner (see Fig. 2). For the weakly compressible formulation the contribution of the hydro-static pressure in the gas phase are neglected, resulting in a discontinuous source term. The piecewise linear interpolation of [26] is extended to include the discontinuous source term

$$\left[\frac{1}{\rho}\frac{\partial p}{\partial x} - \frac{S_g}{\rho}\right]_{\Upsilon} = c \tag{27}$$

Similar to the density, the newly introduced discontinuous source term is computed using a piece-wise constant approximation. Eq. (27) is integrated from node, η, to the edge face, f, to find an expression for p_f in terms of the pressure at node η

$$\int_{\eta}^{f} \frac{1}{\rho}\frac{\partial p}{\partial x} - \frac{S_g}{\rho} dx = \int_{\eta}^{f} c\, dx \tag{28}$$

which yields

$$p_f - p_\eta = \frac{\rho_\eta L}{2}\left(\frac{S_\eta}{\rho_\eta} + c\right) \tag{29}$$

where L is the edge length.

In a similar fashion, by integrating from the edge face, f, to node ξ a face pressure in terms of the pressure and source term at node ξ is obtained

$$p_\xi - p_f = \frac{\rho_\xi L}{2}\left(\frac{S_\xi}{\rho_\xi} + c\right) \tag{30}$$

The face pressure in terms of the pressures and source terms at node η and ξ is found by subtracting Eq. (29) from Eq. (30)

$$p_f = \frac{\rho_\eta p_\xi + \rho_\xi p_\eta}{\rho_\eta + \rho_\xi} + \frac{\rho_\eta \rho_\xi L}{2(\rho_\eta + \rho_\xi)}\left(\frac{S_\eta}{\rho_\eta} - \frac{S_\xi}{\rho_\xi}\right) \tag{31}$$

The extension of the incompressible FSM formulation to account for changes in the density involves the addition of a temporal term to the gas phase. It is found that this may result in a sharp change in the gradient of the velocity over the free-surface interface (as demonstrated in the Numerical evaluation). To ensure an oscillatory free and stable solution, the discretised velocity face flux is interpolated using a non-linear third-order slope limiting scheme. It is found that acceptable results where obtained by employing third-order upwinding with the Sweby limiter ([21]). In this study the extension to unstructured meshes presented by [ ] is used.
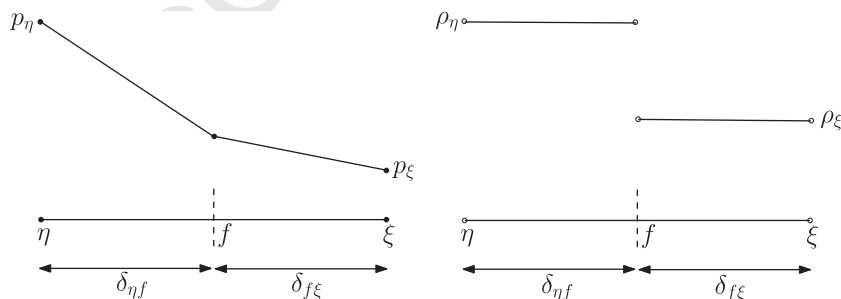

Fig. 2. Interpolation of the edge face values of pressure and density.

4. Numerical evaluation

In this section, the implementation of the proposed weakly compressible formulation is verified by considering test cases with known analytical solutions, where after it is evaluated by means of application focussed problems. The problems considered in the validation of the governing equations describe the expansion and compression of the gas in one- and two-dimensions. In the application focussed test cases the results from the weakly compressible solver are compared to that of an incompressible solver. The material properties are given in Table 1 and the gravitational acceleration of $g = 9.81$ m/s^2 is used.

4.1. Forced compression and expansion of the gas phase

To validate the newly proposed weakly compressible formulation, two test cases which model the forced compression and expansion of a gas pocket are presented. The first considers the linear filling of a quasi one-dimensional tube whereby a gas pocket entrapped at the end of the tube is compressed, whereas, in the second the two-dimensional implementation of the formulation is evaluated by considering the sinusoidal compression and expansion of a gas bubble.

For both cases the analytical solution can be obtained by evaluating the conservation of the liquid and gas mass. It is noted that the liquid density should remain constant as it is assumed to be incompressible and the gas density follows from evaluating the change in volume due to the liquid inflow. The relation between the gas density and pressure is obtained by means of the ideal gas law.

4.1.1. Quasi one-dimensional tube

As mentioned, the first test case considers the linear filling of a quasi one-dimensional tube that is sealed off at the end. Liquid enters the tube at a constant velocity and compresses the entrapped pocket of gas at the end of the tube (Fig. 3). The velocity of the liquid at the inlet is 0.1 m/s and during the 5 s of the analysis, the initial liquid–gas interface propagates from $x = 0.25$ m to $x = 0.75$ m. For the purpose of assessing mesh dependence, three structured meshes are used: A coarse mesh with 3×30 nodes; an intermediate mesh with 3×50 nodes; and a fine mesh with 3×100 nodes. Slip boundary conditions are specified on the sides of the tube and gravity is neglected.

In Fig. 4(a) the averaged pressure in the gas is shown for the three meshes. It shows the non-linear growth in pressure over time and that for the fine mesh the analytical solution is recovered. In Fig. 4(b) the velocity profile for the coarse mesh is shown at various time frames during the analysis ($t = 1$ s, $t = 2$ s, $t = 3$ s and $t = 4$ s). Even for the coarse mesh a good correlation between the numerical and analytical solution is found. Importantly, it is noted that the predicted solution is free of non-physical oscillations, despite the sharp change in the velocity gradient over the free-surface interface. As it is expected, the velocity is constant within the incompressible fluid and reduces linearly in the compressible gas.

4.1.2. Two-dimensional gas bubble

To validate the two-dimensional implementation, a 0.2 m diameter gas bubble subjected to sinusoidal compression and expansion is considered. The bottom of the domain (see Fig. 5) is open and a sinusoidal velocity prescribed

$$u_i = a \sin(2\pi\theta t) \tag{32}$$

where the amplitude and frequency are respectively $a = 0.05$ and $\theta = 2$. As with the previous case, gravity is neglected and slip boundary conditions are specified on the sides of the tube.

Table 1
Material properties for the liquid and gas at 20 °C.

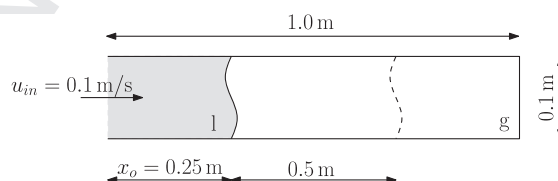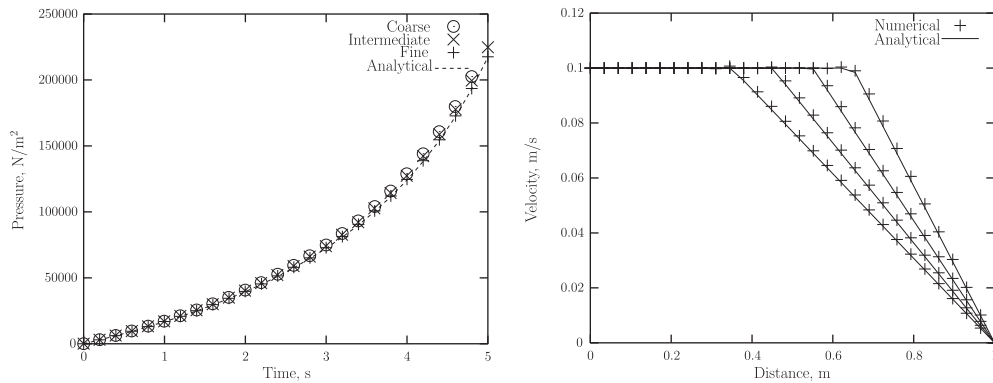|	Liquid (water)	Gas (air)
Density (kg/m^3)	998	1.21
Viscosity (kg/(m s))	1.002×10^{-3}	1.812×10^{-5}
Acoustic velc (m/s)	–	343.2

Fig. 3. Schematic of the quasi one-dimensional tube.

(a) Non-linear increase in the gas pressure   (b) Velocity profile for the coarse mesh at

over time   variations time frames

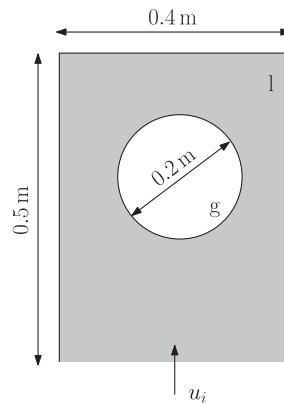**Fig. 4.** Numerical results for the quasi one-dimensional tube.

Fig. 5. Schematic representation of gas bubble.

In Fig. 6(a) the average pressure in the gas bubble is shown. For the analysis three different structured meshes are used with respectively 40×50 nodes, 60×75 nodes, and 80×100 nodes. It is noted that the numerical results of all three meshes very closely approximates the analytical solution, with only a 1.7% difference at the point of highest compression ($t = 0.25$ s). The velocity vectors and bubble contour lines at $t = 0.125$ s are plotted in Fig. 6(b).

4.2. Horizontal shaker

The next test-case involves an application study. For this purpose, a liquid pocket trapped between two gas pockets in a long horizontal tube (Fig. 7) is subjected to variable sideways excitation. The liquid pocket is placed at the centre of the tube and is evaluated under two different horizontal accelerations. In the first analysis, a smooth sinusoidal acceleration is applied to the tube and, in the second, a step function with a sharp ramp in acceleration is applied. These are expressed as

$$a_x^{\sin} = 10 \sin(2\pi t) \tag{33}$$

$$a_x^{\text{step}} = \begin{cases} 0 & \text{if } 0 < t < 0.1 \\ 10 & \text{if } t > 0.1 \end{cases} \tag{34}$$

where a_x is the lateral acceleration and t denotes time. For the purpose of this test case gravitational acceleration as well as the liquid and gas viscosity are neglected.

4.2.1. Sinusoidal excitation

In Fig. 8 the left side wall pressures are plotted over time, where numerical results for different acoustic velocities are compared to an incompressible model. The incompressible model assumes an infinitely large acoustic velocity, which im-
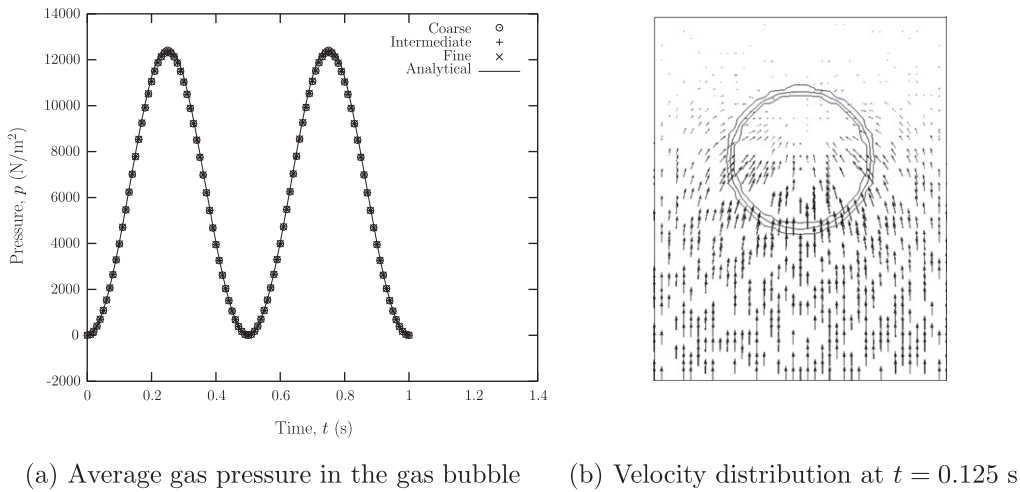
(a) Average gas pressure in the gas bubble   (b) Velocity distribution at $t = 0.125$ s

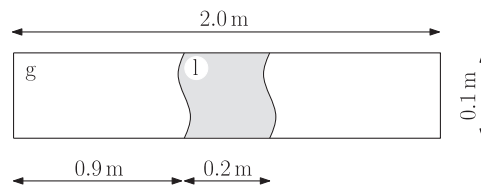**Fig. 6.** Numerical results for the compression and expansion of the gas bubble.

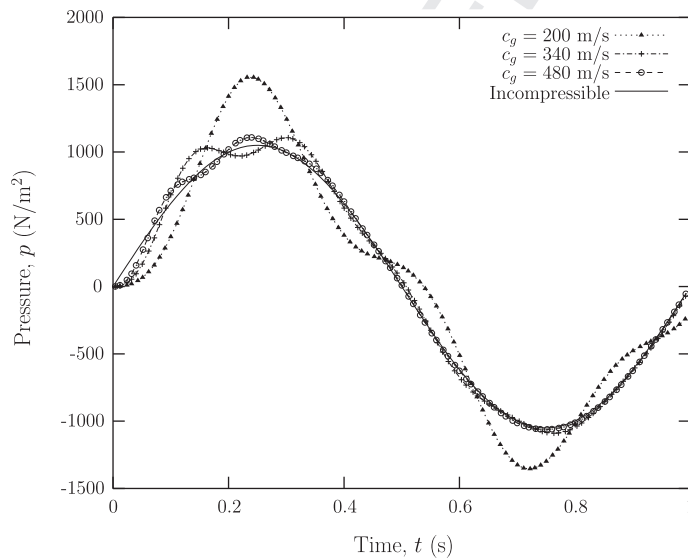**Fig. 7.** Schematic of the entrapped pocket of water under horizontal excitation.

Fig. 8. Left side-wall pressure for the shaker subjected to sinusoidal excitation.

plies no relative liquid–gas movement and the pressure on the side-wall can be approximated as the product of mass times acceleration.

Similar to a spring-mass system, the gas initially absorbs the energy where after it is released, resulting the oscillating behaviour seen in the predicted pressures. From Fig. 8 it is noted that as the gas acoustic velocity increases the numerical solution approaches the incompressible limit. It is found that for the gradual sinusoidal excitation the effect of the compressibility of the gas is less pronounced and the computed maximum pressure is of the same order as the predicted maximum pressure. Only for an acoustic velocity of $c = 200$ m/s a notable difference is present.

4.2.2. Step function excitation

For the liquid pocket subjected to a sharp step-like acceleration the predicted pressures on the left side-wall is show in Fig. 9. The results for different meshes are compared to the analytical solution as well as the incompressible model describe previously. The meshes used for this analysis are refined in the surroundings of the free-surface interface, so that the horizontal spatial resolution in these areas are respectively 0.01 m, 0.005 m and 0.0025 m. For this analysis an acoustic velocity of 343.2 m/s is assumed.

For this problem an analytical solution is obtained by evaluating the forces acting on the liquid pocket. These include the gas pressure acting on the liquid at the left and right liquid–gas interfaces as well as the acceleration of the liquid mass. The gas pressures can be computed in a similar fashion as described in Section 4.1, by considering the conservation of mass. Then by applying the said acceleration to the system, the resulting acceleration of the liquid pocket can calculated and subsequently the relative liquid–gas movement as well as gas density.

From Fig. 9 it is noted that with the sharp step like excitation, the compressibility of the gas greatly influences the pressure measured on the side-wall and the predicted maximum pressure is a factor 2 larger than the pressure predicted by the incompressible model. From the figure it is further noted that as the mesh is refined the numerical results approach the analytical solution. For the coarse mesh where the degree of interface smearing is large compared to the amount of interface movement, it is found that the numerical dissipation fairly quickly dampens out the pressure oscillations, deteriorating the solution accuracy.

In an attempt to quantify the order of the VOF solver along with the weakly compressible extension, the relative L^2 norm error of the left side-wall pressures is shown in Fig. 10. From the figure, it appears the solver is approximately first-order. The order of the solver is influenced by both the spatial non-linear interpolation, which ensures a bounded solution at the numerical discontinuity over the liquid–gas interface, as well as the discretisation of the additional temporal term in the liquid continuity Eq. (14). In Section 3.1 it is noted that the accuracy of the non-linear spatial interpolation varies between first- and second-order accuracy. As the projected pressure Eq. (24), which contains the additional temporal term, is solved in pseudo time it approaches a first-order implicit solution. In this problem where the flow is highly dependent on variations in gas density, the effect of the the first-order approximation of the temporal term is clearly evident.

For large systems subjected to violent sloshing conditions it is not always practical to refine the mesh to the degree stated above, suggesting that these problems will be subjected to poor numerical accuracy. It is, however, noted that for sloshing type analyses the maximum pressure amplitudes and load frequencies are typically of importance and from Fig. 9 it is noted that even with the intermediate mesh acceptable levels of accuracy are obtained during the first oscillation. It is, therefore, suggested that despite these restrictions the weakly compressible FSM formulation provides a measurable improvement in predicting pressure loads of two-fluid flow subjected to irregular accelerations.

4.3. Sloshing analysis of a partially filled tank

Finally, the new weakly compressible formulation is evaluated by means of a comparative study, where a partially filled tank with a baffle configuration under lateral excitation is considered. The tank, shown in Fig. 11, is 70% filled with liquid and is subjected to lateral sinusoidal excitation with an amplitude of 8 m/s^2 and a frequency of 2 Hz. For the analysis a 5000 node structured mesh (see Fig. 11) is used; the pseudo time-step is computed using a CFL number of 0.1 and for the VOF equation the real time step is restricted to a similar Courant number.
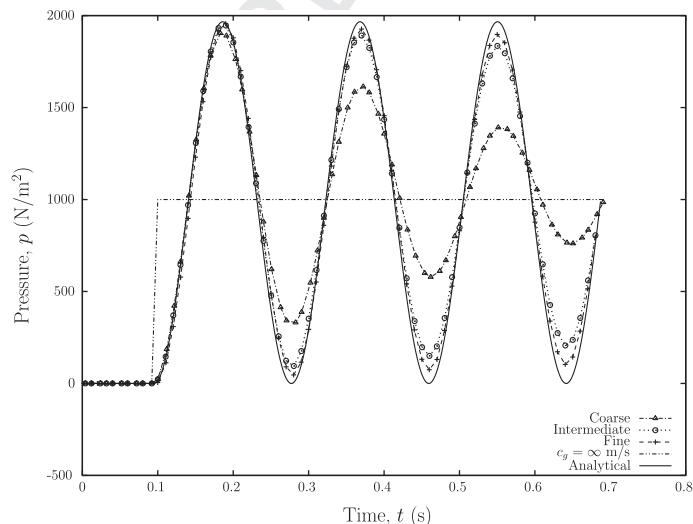

Fig. 9. Left side-wall pressure for the shaker subjected to a step-like function.
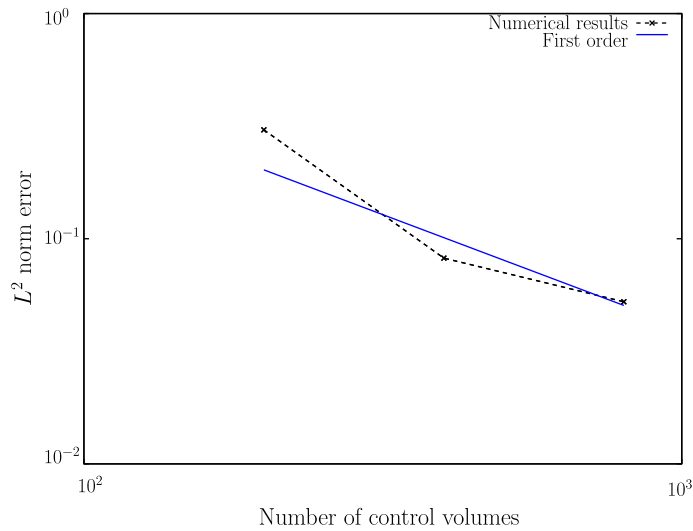
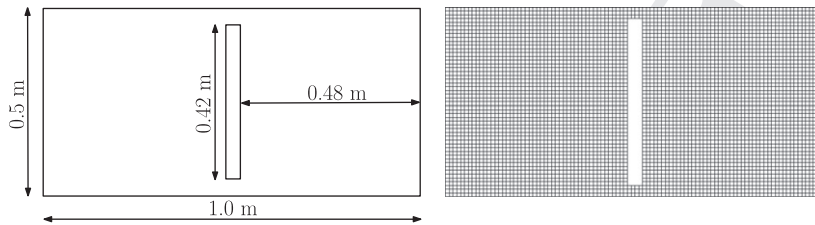**Fig. 10.** Mesh convergence for the horizontal shaker.

Fig. 11. Schematic representation mesh of the tank with baffle subjected to sinusoidal lateral excitation as well as the 5000 node structured mesh.
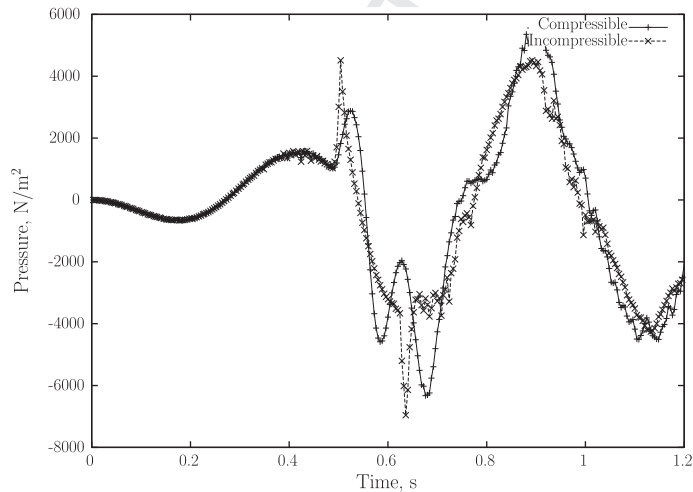

Fig. 12. Difference in average pressure between the left and right side wall of the partially filled tank.

By evaluating the predicted average side-wall pressures, the compressible and incompressible results are compared. As only the change in pressure can be computed for the incompressible flow and not the absolute pressures, the difference between the average left and right side wall pressures is plotted in Fig. 12. The difference between the average pressure measured on the left and right side of the baffle is plotted in Fig. 13.

A notable difference between the compressible and incompressible formulations are the sharp pressure spikes at $t = 0.5$ s and $t = 0.62$ s, which correspond to the times that the top baffle opening is covered by liquid. As the incompressible formu-
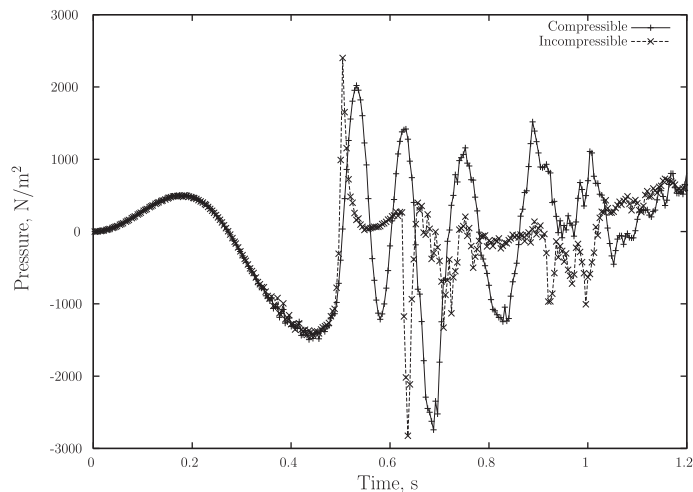
Fig. 13. Difference in average pressure between the left and right baffle walls of the partially filled tank subjected to lateral excitation.

lation is incapable of accounting for the compression of the gas, it results in sharp spikes in the predicted pressure. For the weakly compressible formulation the maximum pressure calculated at these points are slightly less, but as expected, oscillations in pressure are noted as the gas stores and releases energy. Considering the pressures measured on the baffle, it appears the weakly compressible formulation predicts larger variations in the forces acting on the sides as well as an increase in their frequency.

The numerical results seems to indicate the same behaviour as the experimental findings reported by [6–8] which note that the presence of the compressible air may reduce the peak pressure levels, but increases the duration of the impact. For the weakly compressible formulation it is noted that there is a slight improvement in the solution time as the solution converges quicker. As the latter takes into account the compressibility of the gas, it is suspected that the scheme softens the numerical system leading to a quicker convergence of the solution.

5. Conclusion

In conclusion, to take into account the compressible properties of the gas of a low Mach number immiscible liquid–gas system, a new weakly compressible formulation using the VOF approach is developed. Considering liquid–gas systems under low Mach number flow conditions, a new set of governing equations is derived through a non-dimensional analysis. From this it follows that the liquid may be treated as incompressible and the gas modelled using a weakly compressible approximation. The governing equations are implemented in a vertex-centred edge-based solver and the spatial interpolation is done in a manner that ensures an oscillatory free solution. In the application to various test cases the new formulation is validated by demonstrating its capability to accurately represent the compression and expansion of the gas. Furthermore, it is found that the compressible gas has a pronounced effect on pressure predictions for sharp, violent excitation of high density ratio two-fluid flow. In pressure predictions of sloshing analyses it is found that the presence of the compressible gas reduces the peak impact pressures, but increases the duration and frequency of the pressure variations.

References

[1] T. Wacławczyk, T. Koronowiczy, Modelling of the wave breaking with CICSAM and HRIC high-resolution schemes, in: S. Wesseling, E. Oñate, J. Périaux (Eds.), European Conference on Computational Fluid Dynamics ECCOMAS CFD.
[2] D. Liu, P. Lin, Three-dimensional liquid sloshing in a tank with baffles, Ocean Eng. 36 (2009) 202–212.
[3] R. Löhner, C. Yang, E. Oñate, On the simulation of flows with violent free surface motion, Comput. Methods Appl. Mech. Eng. 195 (2006) 5597–5620.
[4] O. Ubbink, R.I. Issa, A method for capturing sharp fluid interfaces on arbitrary meshes, J. Comput. Phys. 153 (1999) 26–50.
[5] D. Lee, M. Kim, S. Kwon, J. Kim, Y. Lee, A parametric sensitivity study on LNG tank sloshing loads by numerical simulations, Ocean Eng. 34 (2007) 3–9.
[6] O. Faltinsen, O. Rognebakke, A. Timokha, Classification of three-dimensional nonlinear sloshing in a square-base tank with finite depth, J. Fluids Struct. 20 (2005) 81–103.
[7] C. Lugni, M. Brocchini, O. Faltinsen, Wave impact loads: the role of the flip-through, Phys. Fluids 18 (2006).
[8] G. Bullock, C. Obhrai, D. Peregrine, H. Bredmose, Violent breaking wave impacts. Part 1: results from large-scale regular wave tests on vertical and sloping walls, Coastal Eng. 54 (2007) 602–617.
[9] M. Liou, L. Nguyen, C. Chang, T. Theofanous, How to solve compressible multifluid equations: a simple, robust and accurate method, AIAA paper 2007, pp. 2007–4456.
[10] A. Murrone, H. Guillard, A five equation reduced model for compressible two phase flow problems, J. Comput. Phys. 202 (2005) 664–698.
[11] E. Romenski, E. Toro, Compressible two-phase flows: two-pressure models and numerical methods, Comput. Fluid Dyn. J. 13 (2004) 403–416.
[12] C. Song, M. Yuan, A weakly compressible flow model and rapid convergence methods, J. Fluids Eng. 110 (1988) 441–455.
[13] W. Chang, L. Lee, H. Lien, J. Lai, Simulations of dam-break flows using free surface capturing method, J. Mech. 24 (2008) 391–403.

[14] M. Bhajantri, T. Eldho, P. Deolalikar, Numerical modelling of turbulent flow through spillway with gated operation, Int. J. Numer. Methods Eng. 72 (2007) 221–243.

[15] C. Song, F. Zhou, Simulation of free surface flow over spillway, J. Hydraul. Eng. 125 (1999) 959–967.

[16] A.G. Malan, J.P. Meyer, R.W. Lewis, Modelling non-linear heat conduction via a fast matrix-free implicit unstructured-hybrid algorithm, Comput. Methods Appl. Mech. Eng. 196 (2007) 4495–4504.

[17] R.W. Lewis, A.G. Malan, Continuum thermodynamic modelling of drying capillary particulate materials via an edge-based algorithm, Comput. Methods Appl. Mech. Eng. 194 (2005) 2043–2057.

[18] Y. Zhao, B. Zhang, A high-order characteristics upwind fv method for incompressible flow and heat transfer simulation on unstructured grids, Comput. Methods Appl. Mech. Eng. 190 (2000) 733–756.

[19] M. Darwish, F. Moukalled, Convective schemes for capturing interfaces of free-surface flows on unstructured grids, Numer Heat Transfer, Part B: Fundam. 49 (2006) 19–42.

[20] S. Muzaferija, M. Perić, P. Sames, T. Schellin, A two-fluid navier-stokes solver to simulate water entry, in: Proc 22nd Symposium on Naval Hydrodynamics, pp. 277–289.

[21] C. Hirt, B. Nichols, Volume of fluid (vof) method for the dynamics of free boundaries, J. Comput. Phys. 39 (1981) 201–225.

[22] F. Dias, D. Dutykh, J. Ghidaglia, A two-fluid model for violent aerated flows, Comput. Fluids 39 (2010) 283–293.

[23] C. Visser, A.G. Malan, J.P. Meyer, An artificial compressibility algorithm for modelling natural convection in saturated packed pebble beds: a heterogeneous approach, Int. J. Numer. Methods Eng. 75 (2008) 1214–1237.

[24] M. Vahdati, K. Morgan, J. Peraire, O. Hassan, A cell-vertex upwind unstructured grid solution procedure for high-speed compressible viscous flow, in: Proceedings at the International Conference on Hypersonic Aerodynamics, Royal Aeronautical Society, London, 1989, pp. 12.1–12.22.

[25] J. Heyns, A. Malan, T. Harms, O. Oxtoby, Development of a compressive surface capturing formulation for modelling free-surface flow by using the volume-of-fluid approach, Int. J. Numer. Methods Fluids (2012).

[26] H. Jasak, H. Weller, Interface tracking capabilities of the inter-gamma differencing scheme, Technical Report, Technical report, CFD research group, Imperial College, London, 1995, 1995.

[27] N. Waterson, H. Deconinck, Design principles for bounded higher-order convection schemes-a unified approach, J. Comput. Phys. 224 (2007) 182–207.

[28] H. Jasak, H. Weller, A. Gosman, High resolution NVD differencing scheme for arbitrarily unstructured meshes, Int. J. Numer. Methods Fluids 31 (1999) 431–449.

[29] P. Nithiarasu, An efficient artificial compressibility (ac) scheme based on the characteristic based split (cbs) method for incompressible flow, Int. J. Numer. Methods Eng. 56 (2003) 1815–1845.

[30] S.V. Patankar, Numerical Heat Transfer and Fluid Flow, McGraw-Hill, New York, 1980.

[31] A.J. Chorin, A numerical method for solving incompressible viscous flow problems, J. Comput. Phys. 2 (1967) 12–26.

[32] A. Malan, R. Lewis, An artificial compressibility cbs method for modelling heat transfer and fluid flow in heterogeneous porous materials, Int. J. Numer. Methods Eng. (2011).

[33] A.G. Malan, R.W. Lewis, P. Nithiarasu, An improved unsteady, unstructured, artificial compressibility, finite volume scheme for viscous incompressible flows: Part I. Theory and implementation, Int. J. Numer. Methods Eng. 54 (2002) 695–714.

[34] A. Malan, O. Oxtoby, A parallel free-surface-modelling technology for application to aircraft fuel-sloshing, in: Lisbon, ECCOMAS CFD-Fifth European Conference on Computational Fluid Dynamics, Lisbon, vol. 14.

[35] H. Luo, D. Sharov, J. Baum R. Löhner Parallel unstructured grid GMRES+LU-SGS method for turbulent flows, AIAA Paper 2003, vol. 273, 2003.

[36] R. Panahi, E. Jahanbakhsh, M. Seif, Development of a vof-fractional step solver for floating body motion simulation, Appl. Ocean Res. 28 (2006) 171–181.

[37] J. Blazek, Computational Fluid Dynamics: Principles and Applications, first ed., Elsevier Science, Oxford, 2001.

[38] Y. Zhao, H.H. Tan, B. Zhang, A high-resolution characteristics-based implicit dual time-stepping vof method for free surface flow simulation on unstructured grids, J. Comput. Phys. 183 (2002) 233–273.